Polish Journal of Medical Physics and Engineering
The Journal of Polish Society of Medical Physics
ISSN 1898-0309, doi: 10.2478/pjmpe-2022-0019

September 2022
Vol 28, Issue 3

Scientific Paper

Physical aspects of Bragg curve of therapeutic oxygen-ion beam: Monte Carlo simulation

Nabil OUNOUGHI [1,ADEF,*], Yamina DRIBI[1,BC], Abdelmalek BOUKHELLOUT[1,BE], Faycal KHARFI[2,EF]

[1]*Radiation Physics and Applications Laboratory, Mohammed Seddik Benyahia University, Jijel, Algeria*
[2]*Laboratory of Dosing, Analysis and Characterization in High Resolution (DAC), Ferhat Abbas Setif1 University, Algeria*
[*]*Corresponding author: Nabil Ounoughi; n_ounoughi@univ-jijel.dz*

(received 28 March 2022; revised 30 July 2022; accepted 10 September 2022)

Abstract

Introduction: Oxygen (^{16}O) ion beams have been recommended for cancer treatment due to its physical Bragg curve feature and biological property. The goal of this research is to use Monte Carlo simulation to analyze the physical features of the ^{16}O Bragg curve in water and tissue.

Material and methods: In order to determine the benefits and drawbacks of ion beam therapy, Monte Carlo simulation (PHITS code) was used to investigate the interaction and dose deposition properties of oxygen ions beam in water and human tissue medium. A benchmark study for the depth–dose distribution of a ^{16}O ion beam in a water phantom was established using the PHITS code. Bragg's peak location of ^{16}O ions in water was simulated using the effect of water's mean ionization potential. The contribution of secondary particles produced by nuclear fragmentation to the total dose has been calculated. The depth and radial dose profiles of ^{16}O, ^{12}C, ^{4}He, and ^{1}H beams were compared.

Results: It was shown that PHITS accurately reproduces the measured Bragg curves. The mean ionization potential of water was estimated. It has been found that secondary particles contribute 10% behind the Bragg peak for ^{16}O energy of 300 MeV/u. The comparison of the depth and radial dose profiles of ^{16}O, ^{12}C, ^{4}He, and ^{1}H beams, shows clearly, that the oxygen beam has the greater deposited dose at Bragg peak and the minor lateral deflection.

Conclusions: The combination of these physical characteristics with radio-biological ones in the case of resistant organs located behind the tumor volume, leads to the conclusion that the ^{16}O ion beams can be used to treat deep-seated hypoxic tumors.

Keywords: Monte Carlo simulation; ion therapy; oxygen ion beam; nuclear fragmentation.

Introduction

Radiation therapy is an efficient cancer treatment technique that uses ionizing radiation to kill tumor cells. As 60 to 70% of all cancer patients require radiotherapy alongside surgery and chemotherapy, this technique is essential for certain cases of treatment.[1] Indeed, the combination of physical and radiobiological properties of radiation beam interaction in tissue is the key to any optimization strategy for this treatment technique.[2-3] Radiation therapy development in terms of clinical practices is essentially due to the important progress in radiation physics, nuclear physics, radiobiology and engineering.

In radiotherapy, charged particles have been established as projectiles of choice that can guarantee many physical and radiobiological benefits than high-energy photons.[4] The main advantage of using charged particles in therapy is their special depth dose distributions in tissue (Bragg curve) which is characterized by a low entrance dose and a narrow peak near the end of the particle's range in the matter known as Bragg peak, BP.[5] In the BP region, charged particle exhibits a high Linear Energy Transfer (LET: unrestricted LET) and higher ionization ability associated with an enhanced Relative Biological Effectiveness (RBE).[6-7] The high LET region can be conformed to cover the 3D geometry of the target, which is more efficient in eradicating certain resistant tumors.[8-9] Today, a multitude of ion beams are produced and accelerated to the desired energy by suitable available accelerators.

Protons and carbon ions are the most effective charged particle radiation used in radiotherapy. Several radiotherapy centers using such beams are in operation around the world and others are under construction or planned for future construction.[10] At Heidelberg Ion-Beam Therapy Center (HIT) center in Germany, the proton and carbon beams have been clinically used since 2009 via an active raster scan method. Since July 2021, the ^{4}He

© 2022 Authors
This is an open access article licensed under the Creative Commons Attribution-NonCommercial-NoDerivs License (http://creativecommons.org/licenses/by-nc-nd/4.0/).

Authors' contribution:
A – Research concept and design, B – Collection and/or assembly of data, C – Data analysis and interpretation, D – Writing the article, E – Critical revision of the article, F – Final approval of the article.

ions beams were started to be used. While ^{16}O ions have so far only been applied for research activities, it is also considered a promising candidate due to their high LET distribution.[11] ^{16}O beams offer a reduced oxygen enhancement ratio (OER) which could be effectively employed to treat hypoxic tumor regions.[12] The first experimental characterization of depth dose distributions of oxygen ion beam was achieved in 2012.[13]

Using the PHITS code Monte Carlo simulation, this work offers an overview of some physical features of a ^{16}O ions beam in a water and tissue phantom. We investigate the capability of PHITS to reproduce experimental data published in the literature on the ^{16}O ions beam depth-dose distributions in a water phantom. We examine the impact of the mean excitation potential of water on the position of BP of the oxygen ion beam. We evaluate the depth-dose of a ^{16}O ion beam in different tissue. Finally, we calculate and compare radial and depth dose profiles of ^{16}O, ^{12}C, ^{4}He, and ^{1}H ions beams (the term "dose" stands for absorbed dose).

Materials and Method

PHITS (Particle and Heavy-Ion Transport code System) is a general-purpose particle and heavy ion 3-dimensional Monte-Carlo radiation transport, which can transport most of the particle species with energies up to 1 TeV/u by using several nuclear reaction models and data libraries.[14] PHITS code has been validated and verified by several applications based on a comparative study of more than fifty irradiation cases.[15] In PHITS (Ver. 3.24) calculation, the Kurotama model[16] was used for the total nucleus-nucleus reaction cross-section, and the JQMD-2.0[17] was used for various aspects of nucleon-induced reactions and heavy-ion interactions, allowing more accurate reproduction of fragmentation cross-sections.

GEM-2.0[18] is used for the light particle's evaporation and fission of the excited residual nuclei stage. Event generator mode (Ver.2) is used in the treatment of low energy transport phenomena below 20 MeV. The EGS5 algorithm was used for simulating the atomic interactions of electrons, positrons, and photons. To consider angular and energy straggling of charged particle, parameters (nspred = 2 nedisp = 1) are used. The energy losses of charged particles except for electrons and positrons are calculated using the ATIMA code with a continuous slowing down approximation. PHITS provides a parameter allowing for user input of the mean ionization potential value of water.

PHITS code has been benchmarked for Bragg curves of ^{1}H, ^{4}He and ^{12}C ion therapy and offers good agreement with calculation and measurements.[19,20] It was used in this work to compute the physical characteristics of the oxygen ion beam.

Results

Sensitivity of the ^{16}O Bragg curves to the mean excitation potential

The mean excitation potential I_w of water, which is used in Bethe–Bloch collision stopping power formula for charged particles, has been recommended by ICRU reports (37, 49, 73) and reported in the literature (measured and calculated).[21] The reported I_w-value range is 67 to 85 eV, which influences the depth dose and BP position of charged particles in water. The PHITS code calculates the stopping power of charged particles using ATIMA, and the ionization potential of water is expected to adjust automatically to 75 eV (ICRU report 37). In the input file, PHITS includes a parameter "ih2o" that allows for an arbitrary input of the mean excitation potential value of water. This option applies to water only. We used PHITS to calculate the Bragg curve with different I_w values to reveal their effect on the ^{16}O Bragg curve in water. We chose a beam with 400 MeV/u energy and changed the value of I_w from 60 eV to 90 eV. The result is represented in **Figure 1**. This simulation demonstrates that changing the value of I_w causes a spatial translation of the ^{16}O ions BP. A 5 eV increase in I_w results in a 1.5 mm increase in range. The value of this parameter has a significant impact on the spatial position of the BP and range, which are both important parameters in treatment planning.

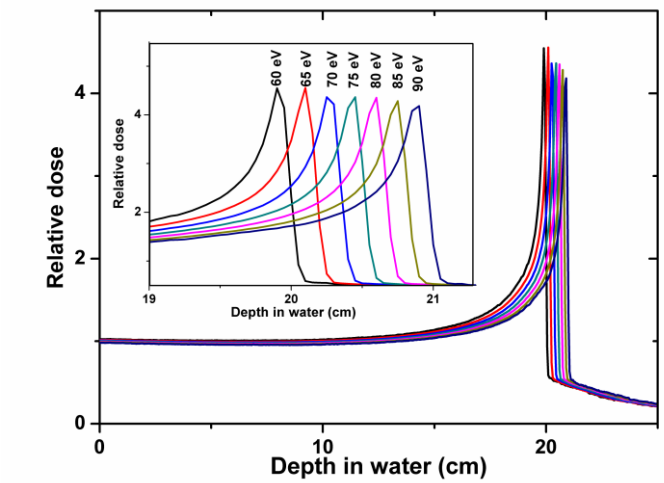


Figure 1. 400 MeV/u ^{16}O ions beam Bragg curve in water at different I_w-values. Statistical uncertainties are below 0.4%

Table 1. Bragg curve parameters of a ^{16}O beam in water for energies of 129.65, 300.13, and 430.32 MeV/u.

Incident energy (MeV/u)	Beam FWHM (mm)	R_{80} Exp	R_{80} PHITS I_w= 75 eV	R_{80} PHITS I_w= 79.5 eV	R_{80} PHITS I_w= 78 eV
129.65	8.4	3.07	3.05	3.07	3.06
300.13	4.3	12.91	12.84	12.93	12.90
430.32	3.6	23.14	23.04	23.19	23.14

Benchmarking of PHITS for ^{16}O Bragg curve in the water phantom

The depth-dose distributions of a ^{16}O beam in a water phantom are simulated with PHITS and compared to published experimental results obtained at the Heidelberg Ion-Beam Therapy Center in this study. Kurz et al.[13] describe the experimental system and setup, where three initial pencil beam energies were chosen with full widths at half maximum FWHM of 129.65, 300.13, and 430.32 MeV/u, as shown in **Table 1**. By adding the water equivalent thickness of all nozzle elements, the absolute depth dose in water was optioned. The position of the Bragg peak and the shape of the Bragg curve can both be sensitive to water's mean excitation potential. The experimental Bragg curve was optimized and adjusted to 79.5 eV for water ionization potential.[13]

In our simulation, a simple cylindrical phantom of water with a radius of 5 cm and a height of 30 cm is utilized in the PHITS simulation (experimental geometry). The deposited energy was scored in smaller cylinders with a radius of 4 cm and a height of 0.05 cm, with a calculated standard deviation of less than 0.4 %. **Figure 2** illustrates the simulated and measured depth-dose distributions for all three energies investigated, normalized to the entrance.

It was shown that PHITS accurately reproduces the shape of the measured Bragg curves. The depth where the dose falls to 80% at the peak value is described as the range of ^{16}O ions in water (R_{80}). Ranges of ^{16}O estimated by PHITS at various energies for various values of I_w are compared to experimental data (R_{80} Exp) given in.[22] **Table 1** summarizes the results. The experimental results are reported to be more similar to those obtained for I_w = 78 eV (ICRU report 90) than for I_w = 79.5 eV.

Contribution of secondary fragments to dose deposition of oxygen beam

When a primary ^{16}O ion passes through a medium, the target and projectile nuclei are subjected to nuclear fragmentation. Secondary fragments are produced along the penetration path and contribute to the total dose.[23] The PHITS code can also calculate dose profiles for primary and secondary particles; more benchmark results on PHITS fragments production cross-sections of ^{16}O are provided in reference [24]. We compute the deposited energy by the oxygen beam and the secondary particles produced by the fragmentation reaction in the water phantom. The calculated contributions to the total depth-dose from the primary ^{16}O ion beam and secondary particles, as well as experimental data for incoming energy of 300.13 MeV/u, are shown in **Figure 3**. The Bragg curve shape and secondary fragments dose beyond the Bragg peak are very well reproduced.

The dose behind the BP is only due to the secondary particle created by nuclear fragmentation after the interaction of ^{16}O incident ions with atoms of the water phantom; their contribution is about 10% of the total dose.

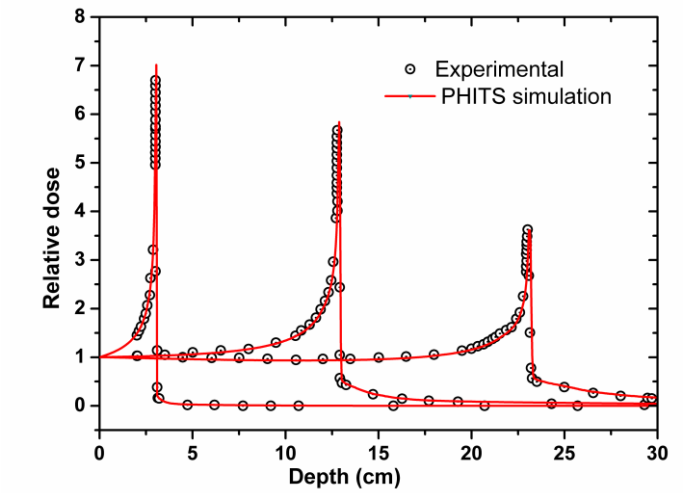


Figure 2. Bragg curves of ^{16}O ion beams at three energies (129.7, 300.13 and 403.31 MeV/u) in a water phantom as predicted by PHITS. Statistical uncertainties are below 0.4%. Experimental data are taken from reference [13].

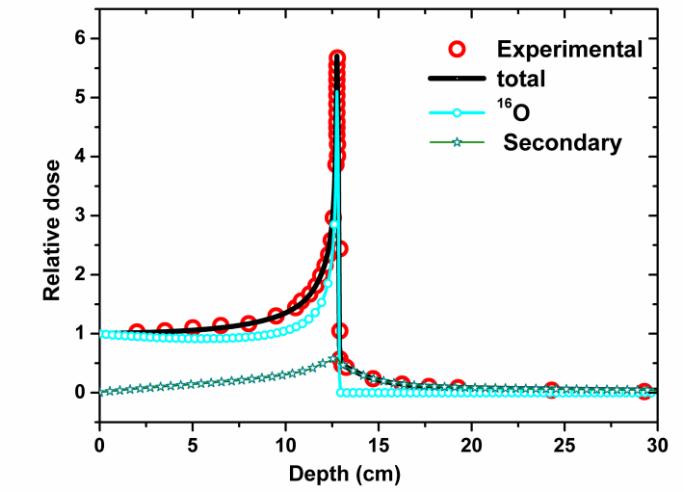


Figure 3. Calculated Bragg curves for 300.13 MeV/u ^{16}O in water, together with contributions from the primary ^{16}O ions and secondary fragments. Statistical uncertainties are below 0.4%. Experimental data are taken from reference [13].

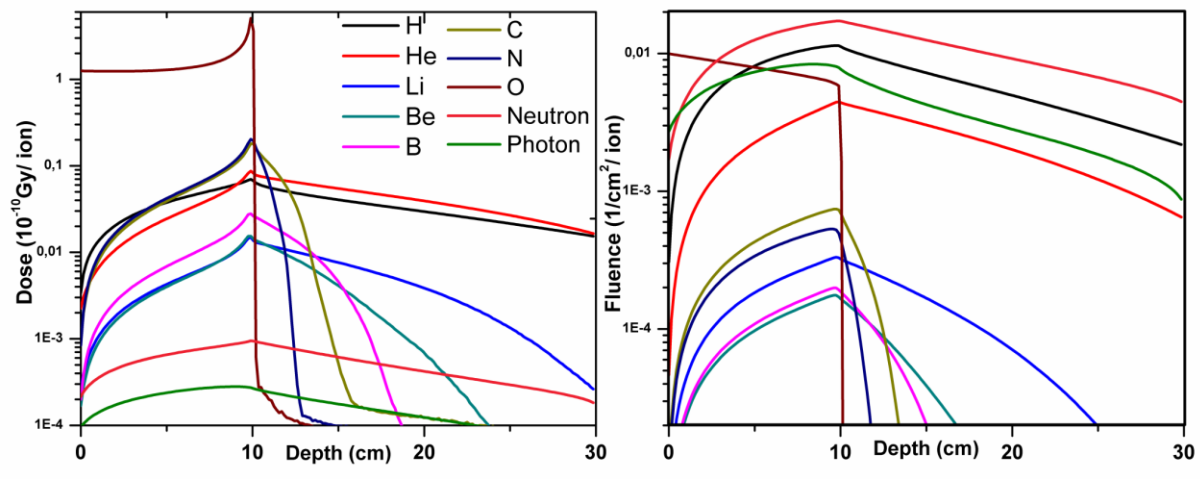


Figure 4. Physical dose (left side) and fluence (right side) of primary ^{16}O and secondary fragments as predicted with PHITS for 259.6 MeV/u ^{16}O in water. Statistical uncertainties are below 1%.

Nuclear fragmentation generates energetic low-atomic-number (Z < 8) Hydrogen, Helium, Lithium, Beryllium, Boron, Carbon, and Nitrogen fragments with a range longer than the primary ^{16}O ions, which deposit their energy after the BP.[25] During the interaction of ^{16}O ions, neutrons and photons are also produced and travel beyond the BP in addition to light ions. In previous work, we estimated the secondary neutron contribution in the soft tissue phantom for an ^{16}O ion beam.[26] The undesirable tail and lateral dose caused by fragmentation complicate the treatment control. A better understanding of the fragmentation phenomenon would enable more precise dose delivery control in healthy tissues.

Characterization of secondary particle field

Secondary fragments created by the interaction of the primary ^{16}O beam induce some additional physical and biological effects. To estimate these effects, it is necessary to determine the distribution of the primary and secondary particles at a given penetration depth. **Figure 4** shows computed physical dose and fluence of primary oxygen ion and secondary fragments as a function of depth as calculated with PHITS code by considering a water phantom as dose deposition medium.

As it can be easily checked at the BP position level, the largest contribution in dose deposition is due to C and N fragments. H and He contribute less in dose deposition at this position. Beyond the BP position, the dose deposition is the sum of the contributions of different lower-Z fragments. Indeed, H and He are the main contributors because they have a longer range than primary oxygen ions showing therefore a long dose tail behind the BP. Li, Be and B fragments contribute lightly to dose deposition.

Fragmentation of the oxygen beam upon entering the tissue phantom can produce many isotopes of species with Z less than 8 (^{15}O, ^{14}N, ^{13}N, ^{12}N, ^{14}C, ^{13}C, ^{12}C, ^{11}C, ^{10}C, ^{11}B, ^{10}B,^{10}Be, ^{9}Be, ^{7}Be, ^{7}Li, ^{6}Li, ^{4}He, ^{3}He, ^{3}H, ^{2}H, ^{1}H) with different production cross sections.[27]

The ^{11}C, ^{15}O, ^{10}C and ^{13}N are also among the most important positron emitters created isotopes with half-life of 20.33 min, 122 s, 19.31 s and 9.97 min, respectively. In addition to their use as treatment beam, ^{16}O ions and particularly some of their created fragments, such as the above-mentioned radioisotopes can be used for the in vivo verification of the treatment planning. Such verification is ensured by Positron Emission Tomography imaging (PET) through the determination of the spatial distribution of the produced positron emitters. Such additional application can be ensured if the treatment machine is equipped with a PET imaging SYSTEM. In this work, a Monte Carlo with PHITS code was performed to predict the possible positron emitters that can be created in soft tissue during ^{16}O irradiation. **Figure 5** shows that the fluency of the ^{15}O positron emitter radioisotope is higher than the other radioisotopes. Because of its short half-life, ^{15}O is the best-adapted positron emitter for PET imaging that may guarantee a short scanning time.[28]

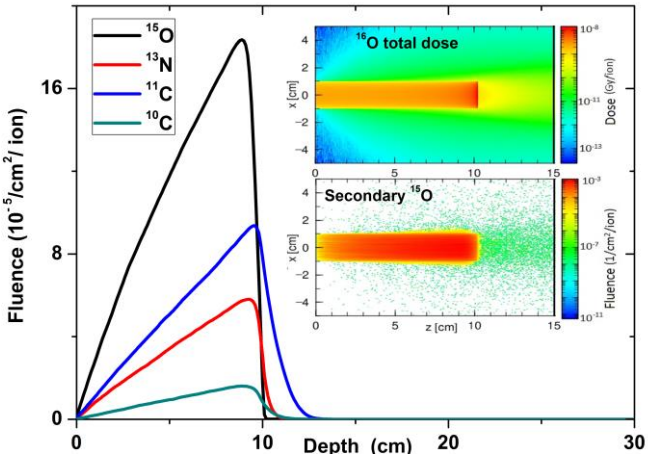


Figure 5. Fluence of the main positron emitters during the interaction of ^{16}O ions of energy 259.6 MeV/u in a water phantom as predicted with PHITS. The inset shows 2D map of the total dose and fluence of secondary ^{15}O (diameter of the beam is 2 cm). Statistical uncertainties are below 1%.

Recently, oxygen ions have been considered a potential alternative to carbon ions. When compared to carbon ions, oxygen ions have a high LET.[29] The dose averaged LET (LET-dose) plays a key role in accounting for biological effectiveness.[30] This principal average takes into account the contribution of each type fragment; it is highly dependent on the secondary particle spectrum. **Figure 6** shows the dose averaged LET as calculated with PHITS for ^{16}O and ^{12}C at respectively energy 259.6 and 218.8 MeV/u in a water phantom. It is clear that dose-averaged LET is higher for ^{16}O to ^{12}C at BP. Higher LET, would also cause a significant reduction of the OER. The reduction of OER values with increasing LET of the particle is designated in [31].

Beyond the BP, the dose contribution of the secondary particle is higher with incoming ^{16}O ions than ^{12}C ions. **Figure 7** shows the comparison of the secondary fragment, neutron and photon dose produced by ^{16}O and ^{12}C ions in the water phantom. The result of comparison is performed by PHITS at respectively energy 259.6 and 218.8 MeV/u. Compared to ^{12}C ions, ^{16}O ions have a higher dose beyond BP and create more neutrons and photons.

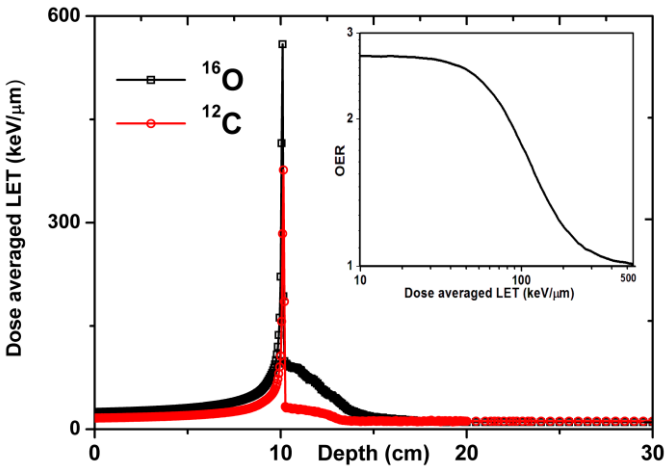


Figure 6. Dose averaged LET as calculated with PHITS for ^{16}O and ^{12}C at respectively energy 259.6 MeV/u and 218.8 MeV/u in water. The inset shows the distribution of OER as a function of dose averaged LET (Data taken from reference [31]).

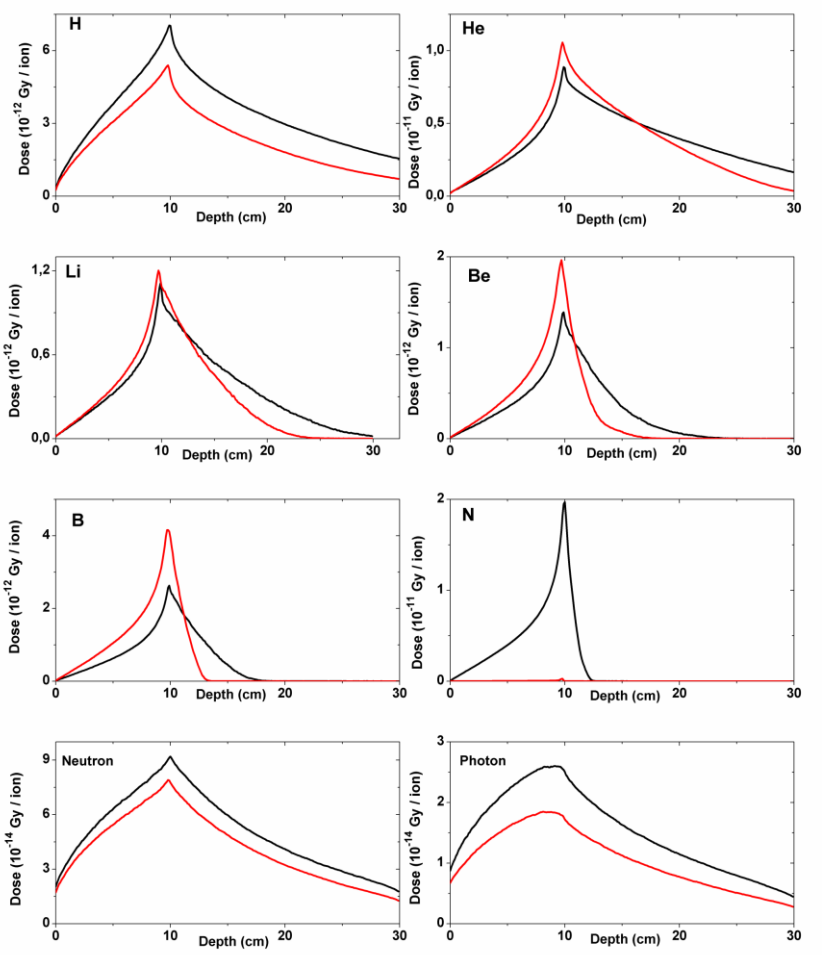


Figure 7. Comparison of depth dose distribution curves produced by secondary particles, for incident oxygen (black) and carbon (red) ion beams with energy 259.6 MeV/u and 218.8 MeV/u, respectively.

Oxygen beam at different incoming beam energy in tissue phantom

To show the effect of incoming beam energy on the Bragg curve, we performed a simulation on the interaction of a ^{16}O ion beam in a soft tissue phantom with different initial energies ranging from 200 to 430 MeV/u (energies of interest for radiotherapy applications). The soft tissue is composed of four elements, ICRU Report 44,[32] with densities (1 g/cm^3) and weight fractions as follows: H (0.762), C (0.111), O (0.10), and N. (0.026). The mean ionization potential is 74.9 eV. The results of the calculation are shown in **Figure 8**.

The results show that as the incoming beam energy increases, the BP position is translated to deeper parts of soft tissue and their amplitude decreases. As a result, the peak-to-entrance dose ratio is lowest at high energies and increases as energy decreases. This is due to the enlargement of the Bragg Peak caused by straggling effects at deeper depths. **Table 2** shows that increasing the incoming beam energy increases the longitudinal $FWHM_L$ at BP value.

The depth dose of the ^{16}O ion beam was calculated using PHITS at incoming energies of 200 and 400 MeV/u in four targets (soft tissue, compact bone, brain, and adipose tissue). The composition of human tissues and their mean excitation potential values were obtained from ICRU Report 44. The results are represented in **Figure 9**.

Table 3 shows the density and means ionization energy of four targets used in the simulation, and the location of BP at 200 MeV/u (BP_{200}) and 400 MeV/u (BP_{400}). As the energy of the primary ion increased from 200 to 400 MeV/u, the BP position was moved to the deeper parts of the target about 8.1, 13.4, 14 and 14.9 cm, respectively for bone, brain, soft tissue, and adipose tissue. The four targets revealed a reduction dose ratio by ~2.3 with the increase in incident ion energy from 200 to 400 MeV/u.

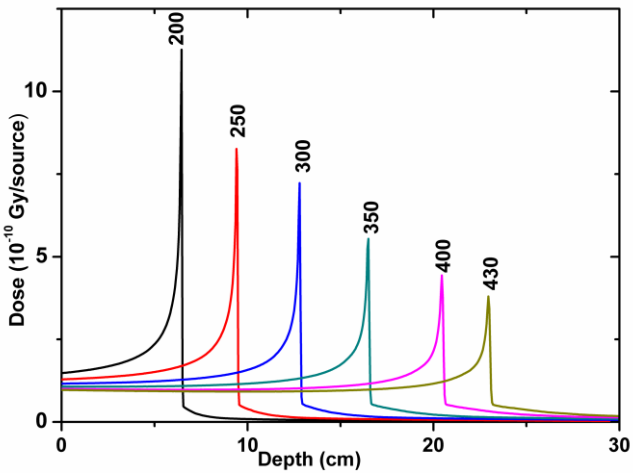


Figure 8. Bragg curve of ^{16}O ion beam in soft tissue at different incoming energy (200 to 430 MeV/u). Data normalized to one source particle. Statistical uncertainties are below 1%.

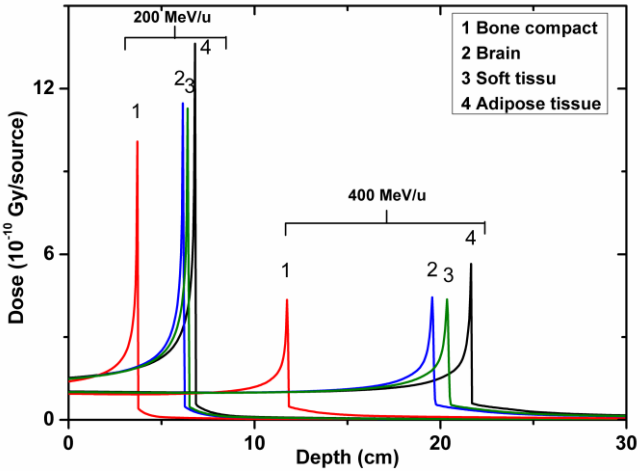


Figure 9. Bragg curve of ^{16}O ion beam in four types of tissue, at 200 and 400 MeV/u. Data normalized to one source particle. Statistical uncertainties are below 1%.

Table 2. Bragg curve characteristics of a ^{16}O in soft tissue at different incoming energy (200 to 430 MeV/u). (P/E : Peak-to entrance ratio).

Energy (MeV/u)	BP location (cm)	$FWHM_L$ (mm)	P/E
200	6.45	2.0	7.6
250	9.4	2.5	6.5
300	12.8	3.0	5.7
350	16.5	4.5	5.1
400	20.45	5.0	4.5
430	22.95	6.0	3.9

Table 3. Location in depth of Bragg peak at 200 MeV/u (BP200) and 400 MeV/u (BP400) in different tissue (mass density: ρ mass density, I: main ionization potential).

Tissue	ρ[g/cm^3]	I [eV]	BP_{200} location [cm]	BP_{400} location [cm]
Bone compact	1.85	91.9	3.70	11.75
Brain	1.03	73.3	6.15	19.55
Soft tissue	1	74.9	6.40	20.35
Adipose tissue	0.92	63.2	6.80	21.65

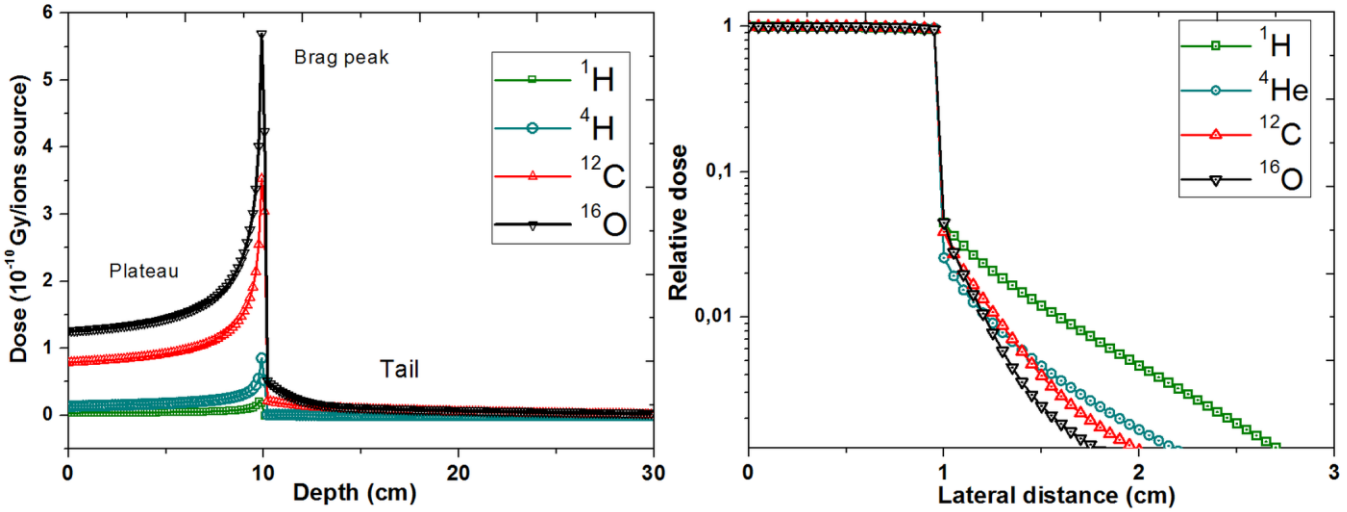


Figure 10. Calculated Bragg curves (left side) and normalized radial dose profiles at BP (right side) in water for ^{1}H, ^{4}He, ^{12}C and ^{16}O ions. Statistical uncertainties are below 1%.

Depth and lateral dose distributions of ^{16}O, ^{12}C, ^{4}He, and ^{1}H ion beams

Monte Carlo simulation of dose distribution of therapeutic ion beams of ^{16}O, ^{12}C, ^{4}He, and ^{1}H gives a review to compare their use in ion radiotherapy. In the Bragg curve of charged particles, the depth position of the BP depends on the nature of the medium, the type and the initial energy of the ion beam used. In this study, the incoming energy of ^{16}O, ^{12}C, ^{4}He, and ^{1}H beams are chosen respectively 258, 217.5, 115.5, and 115 MeV/u. For each ion, these energies have the same range in water (10 cm). The depth-dose and radial dose distribution for different ions in water phantom calculated with PHITS code are shown in **Figure 10**.

By comparison, oxygen beams induced a dose per incident ion slightly higher than that of carbon, but a significant difference was observed compared with helium and proton. However, a remarkable dose was observed in the plateau and tail regions of the oxygen and carbon ions beams. The observed tail in dose deposition is due to the nuclear fragmentation processes of the primary ^{12}C ion and ^{16}O ion during their nuclear interactions with the atoms of the irradiated water phantom (left-hand side of **Figure 10**). This physical phenomenon affects the characteristics of the primary ion beam and must be taken into account in dose calculation and treatment planning in the case of ion beam therapy.

Simulation of radial profiles of the physical dose at BP for different kinds of ions (right-hand side of **Figure 10**) shows that the oxygen beam presents a small lateral deflection in comparison to the proton. This interesting property provides a clinical advantage for oxygen ions in the treatment of tumors when organs at risk are located laterally to the direction of the beam. **Figure 11** shows the 2D spatial depth dose distribution (Gray per incident ion) of a cylindrical beam (2 cm diameter) of different ions in a water phantom.

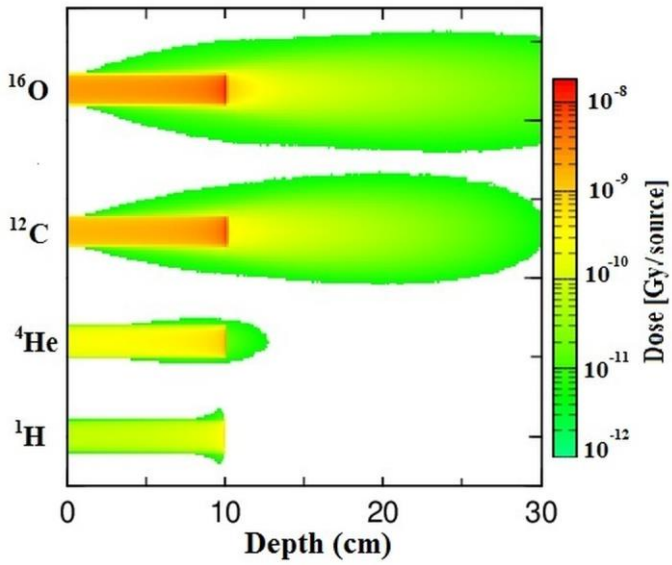


Figure 11. 2D depth dose distribution of different ions (a cylindrical beam of 2 cm diameter). Data normalized to one source particle.

This indicates that ^{12}C ion and ^{16}O ion beams are not recommended for use if very sensitive organs are located behind the tumor volume but ^{1}H and ^{4}He are suitable. Tommasino et al.[33] have discussed the potential and limitations of those four type of particle species in ions therapy.

Discussion

The major advantage behind using charged particles as an effective hadron therapy is their very suitable depth dose distribution in tissues in case of the treatment of certain radio-resistant tumor that requires a high LET for their eradication. Although protons and carbon ^{12}C ions have been already and effectively used for the treatment of deep-seated radio-resistant tumors, ^{16}O is, actually, considered a new alternative that brings some additional benefits to radiation therapy. In this paper, Monte Carlo simulation with PHITS code was used to study

various physical features of oxygen ions beam in water and tissue equivalent phantom. The main objective of this work is to demonstrate some advantages and disadvantages when using such ions in radiotherapy. In this study, PHITS code has been benchmarked for the Bragg curve of ^{16}O ions beams in water for three energies within the therapeutic energy range. The effect of the mean excitation potential is discussed and Bragg curves for some tissues of interest are simulated. The secondary particles generated by the fragmentation phenomena are calculated. These particles were found to be the major actor in dose deposition behind the Bragg peak position. The Bragg curves of ^{16}O ions beam were calculated and compared in cases of different tissues with various incoming energies. The comparison of computed depth and radial dose distributions of ^{1}H, ^{4}He, ^{12}C and ^{16}O shows that ^{16}O ions produced the higher dose at the Bragg peak position and a small lateral deflection. The main disadvantage in using ^{16}O beam in radiotherapy is due to some problems of dose conformity and coverage due to the importance of the nuclear fragmentation process that may induce uncontrolled isodose surface of the target volume in the case of some kind of tumors. Indeed, ^{16}O fragments are responsible for dose deposition beyond the Bragg peak and out-of-field. With such dose deposition characteristics due to fragmentation, the treatment, when sensitive organs at risk are situated at the distal edge, will seriously compromise the treatment planning. Finally, if we disregard the problem that we have just mentioned that can be tolerated in some treatment cases, the studied dose deposition and radiobiological features of ^{16}O ions beam demonstrate well that such ions constitute a serious alternative to treat deep-seated radio-resistant tumor in the case of resistant organs located behind the tumor.

Conclusion

The higher LET of the oxygen ^{16}O beam, which has been shown to be the key to overcoming tumor hypoxia, has given them a viable alternative to ^{12}C. Another advantage of ^{16}O for radiotherapy is its low lateral deviation, which may be useful in the treatment of tumors located laterally to the beam. The disadvantage of using a ^{16}O beam in radiotherapy is that it accelerates the nuclear fragmentation process, resulting in a higher production of nuclear fragments, which complicates treatment when sensitive organs are located at the distal edge. Finally, in the case of resistant organs located behind the tumor, the combination of those physical characteristics with radiobiological ones, ^{16}O ion constitutes a serious alternative to treat deep-seated hypoxic tumor.

Acknowledgments

We like to thank the Algerian Ministry of Higher Education and Scientific Research and the DGRSDT for supporting partially this work.

References

1. Raj V, Rai A, Sharma S, et al. Role of synchrotron radiation in cancer: A review on techniques and applications. J Anal Pharm Res. 2018;7(2):175-180. https://doi.org/10.15406/japlr.2018.07.00221
2. Baskar R, Lee KA, Yeo R, et al. Cancer and radiation therapy: current advances and future directions. Int J Med Sci. 2012;9(3):193-199. https://doi.org/10.7150/ijms.3635
3. Scaife JE, Barnett GC, Noble DJ, et al. Exploiting biological and physical determinants of radiotherapy toxicity to individualize treatment. The British Journal of Radiology. 2015;88:1051. https://doi.org/10.1259/bjr.20150172
4. Schardt D, Elsässer T, Schulz-Ertner D. Heavy-ion tumor therapy: Physical and radiobiological benefits. Rev Mod Phys. 2010;82:383-425. https://doi.org/10.1103/RevModPhys.82.383
5. Ugo A, Gerhard K. Radiotherapy with beams of carbon ions. Rep Prog Phys. 2005;68(8):1861-1882. https://doi.org/10.1088/0034-4885/68/8/R04
6. Kantemiris I, Karaiskos P, Papagiannis P, et al. Dose and dose averaged LET comparison of ^{1}H, ^{4}He, ^{6}Li, ^{8}Be, ^{10}B, ^{12}C, ^{14}N, and ^{16}O ion beams forming a spread-out Bragg peak. Med Phys. 2011;38(12):6585-6591. https://doi.org/10.1118/1.3662911
7. Hamdi DH, Barbieri S, Chevalier F, et al. In vitro engineering of human 3D chondrosarcoma: a preclinical model relevant for investigations of radiation quality impact. BMC Cancer. 2015;15:579. https://doi.org/10.1186/s12885-015-1590-5
8. Durante M, Orecchia R, Loeffler JS. Charged-particle therapy in cancer: clinical uses and future perspectives. Nat Rev Clin Oncol. 2017;14(8):483-495. https://doi.org/10.1038/nrclinonc.2017.30
9. Hamdi DH, Chevalier F, Groetz JG, et al. Comparable Senescence Induction in Three-dimensional Human Cartilage Model by Exposure to Therapeutic Doses of X-rays or C-ions. Int J Radiat Oncol Biol Phys. 2016;95(1):139-146, https://doi.org/10.1016/j.ijrobp.2016.02.014
10. Particle Therapy Facilities in Clinical Operation. Accessed: January 2022. [Online]. Avalable: https://www.ptcog.ch/index.php/facilities-in-operation

11. Lysakovski P, Ferrari A, Tessonnier T, et al. Development and Benchmarking of a Monte Carlo Dose Engine for Proton Radiation Therapy. Front Phys. 2021;9:741453. https://doi.org/10.3389/fphy.2021.741453
12. Sokol O, Scifoni E, Tinganelli W, et al. Oxygen beams for therapy: advanced biological treatment planning and experimental verification. Phys Med Biol. 2019;62(19):7798-7813. https://doi.org/10.1088/1361-6560/aa88a0
13. Kurz K, Mairani A, Parodi P. First experimental based characterization of oxygen ion beam depth dose distributions at the Heidelberg ion beam therapy center. Phys Med Biol. 2012;57(15):5017-5034. https://doi.org/10.1088/0031-9155/57/15/5017
14. Sato T, Kase Y, Watanabe R, et al. Biological Dose Estimation for Charged-Particle Therapy Using an Improved PHITS Code Coupled with a Microdosimetric Kinetic Model. Radiation Research. 2009;171(1):107-117. https://doi.org/10.1667/RR1510.1
15. Iwamoto Y, Sato T, Hashimoto S, et al. Benchmark study of the recent version of the PHITS code. Journal of Nuclear Science and Technology. 2017;54(5):617-635. https://doi.org/10.1080/00223131.2017.1297742
16. Iida K, Kohama A, Oyamatsu K. Formula for Proton-Nucleus Reaction Cross Section at Intermediate Energies and Its Application. J Phys Soc Jpn. 2007;76(4):04420. https://doi.org/10.1143/JPSJ.76.044201
17. Ogawa T, Sato T, Hashimoto S, et al. Energy-dependent fragmentation cross sections of relativistic C12. Phys Rev C. 2015;92:024614. https://doi.org/10.1103/PhysRevC.92.029904
18. Furihata M, Statistical analysis of light fragment production from medium energy proton-induced reactions. Nucl Instrum Methods Phys Res B. 2000;171:251-258. https://doi.org/10.1016/S0168-583X(00)00332-3
19. Puchalska M, Tessonnier T, Parodi K, et al. Benchmarking of PHITS for Carbon Ion Therapy. Int J Part Ther. 2018;4(3):48-55. https://doi.org/10.14338/IJPT-17-00029.1
20. Parisi A, Nascimento LF, Van Hoey O, et al. Low temperature thermoluminescence anomaly of LiF:Mg,Cu,P radiation detectors exposed to ^{1}H and ^{4}He ion. Radiation Measurements. 2018;119:155-165. https://doi.org/10.1016/j.radmeas.2018.10.008
21. Soltani-Nabipour J, Sardari D, Cata-Danil G. Sensitivity of the bragg peak curve to the average ionization potential of the stopping medium. Rom Jurn of Phys. 2009;54(3-4):321-330.
22. Resch, AF, Fuchs, H, Georg D. Benchmarking GATE/Geant4 for ^{16}O ion beam therapy. Phys Med Biol. 2017;62(18):N474-N484. https://doi.org/10.1088/1361-6560/aa807e
23. MacCabee HD, Ritter MA. Fragmentation of High-Energy Oxygen-Ion Beams in Water. Radiation Research. 1974;60(3):409-421. https://doi.org/10.2307/3574021
24. Zeitlin C, Miller J, Guetersloh S, et al. Fragmentation of ^{14}N, ^{16}O, ^{20}Ne, and ^{24}Mg nuclei at 290 to 1000 MeV/nucleon. Physical Review C. 2011;83(3):034909. https://doi.org/10.1103/PhysRevC.83.034909
25. Rucinski A, Traini, G, Roldan, AB, et al. Secondary radiation measurements for particle therapy applications: Charged secondaries produced by ^{16}O ion beams in a PMMA target at large angles. Physica Medica. 2019;64:45-53. https://doi.org/10.1016/j.ejmp.2019.06.001
26. Boukhellout A, Ounoughi N, Kharfi F. Monte-Carlo simulation using PHITS of secondary neutrons produced in-patient during ^{16}O ion therapy. Radiat Prot Dosimetry. 2022;198(1-2):31-36. https://doi.org/10.1093/rpd/ncab188
27. Ogawa T, Sato S, Hashimoto S, et al. Analysis of multi-fragmentation reactions induced by relativistic heavy ions using the statistical multi-fragmentation model. Nucl Instrum Methods Phys Res A. 2013;723:36-46. https://doi.org/10.1016/j.nima.2013.04.078
28. Grogg K, Alpert NM, Zhu X, et al. Mapping ^{15}O production rate for proton therapy verification. Int J Radiat Oncol Biol Phys. 2015;92(2):453-459. https://doi.org/10.1016/j.ijrobp.2015.01.023
29. Ying C K, Bolst D, Rosenfeld A, et al. Characterization of the mixed radiation field produced by carbon and oxygen ion beams of therapeutic energy: A Monte Carlo simulation study. J Med Phys. 2019;44:263-269. https://www.jmp.org.in/text.asp?2019/44/4/263/272671
30. Grzanka L, Ardenfors O, Bassler N. Monte Carlo simulations of spatial let distributions in clinical proton beams. Radiation Protection Dosimetry. 2018;180(1-4):296-299 https://doi.org/10.1093/rpd/ncx272
31. Tinganelli W, Durante M, Hirayama R, et al. Kill-painting of hypoxic tumours in charged particle therapy. Sci Rep. 2015;5:17016. https://doi.org/10.1038/srep17016
32. ICRU, 1989. Tissue substitutes in radiation dosimetry and measurement. Report 44, International Commission on Radiation Units and Measurements, Bethesda, MD, USA.
33. Tommasino F, Scifoni E, Durante M. New ions for therapy. International Journal of Particle Therapy. 2016;2(3):428-438. https://doi.org/10.14338/IJPT-15-00027.1